Integrative Biology

Accepted Manuscript

ROYAL SOCIETY OF CHEMISTRY

www.rsc.org/ibiology

Insight Box

Epithelia must preserve their barrier integrity despite a variety of challenges that include cell death, infection, cell division and injury. In particular, these processes affect a small numbers of cells and their surrounding neighbours reorganize in order to preserve tissue integrity. In this work, we used theoretical approximations and simulations to analyse the biomechanical properties of cell-cell junctions during these dynamic rearrangements. Moreover, we also determined the relationship between adhesion and contraction that allow cells to efficiently remodel their cell-cell junctions in response to injury. Overall, our results suggest that at the sites of cell-cell adhesion, changes in the balance between contraction and adhesion is required for wound closure to occur.

Modelling wound closure in an epithelial cell sheet using the Cellular Potts Model

Adrian Noppe[a], Anthony P. Roberts[a], Alpha S. Yap[b], Guillermo A. Gomez[b] and Zoltan Neufeld[a,b]

June 5, 2015

Author Affiliations: [a]School of Mathematics and Physics and [b]Institute for Molecular Bioscience, Division of Cell Biology and Molecular Medicine, The University of Queensland, St. Lucia, Brisbane, Queensland, Australia 4072

Abstract

We use a two-dimensional Cellular Potts Model to represent the behavior of an epithelial cell layer and describe its dynamics in response to a microscopic wound. Using an energy function to describe properties of the cells, we found that the interaction between contractile tension along cell-cell junctions and cell-cell adhesion plays an important role not only in determining the dynamics and morphology of cells in the monolayer, but also in influencing whether or not a wound in the monolayer will close. Our results suggest that, depending on the balance between cell-cell adhesion and junctional tension, mechanics of the monolayer can either correspond to a hard or a soft regime that determines cell morphology and polygonal organization in the monolayer. Moreover, the presence of a wound in a hard regime, where junctional tension is significant, can lead to two results: 1) wound closure or 2) an initial increase and expansion of the wound area towards an equilibrium value. Theoretical approximations and simulations allowed us to determine the thresholds in the values of cell-cell adhesion and initial wound size that allow the system to lead to wound closure. Overall, our results suggest that around the site of injury, changes in the balance between contraction and adhesion determine whether or not non-monotonous wound closure occurs.

1 Introduction

Epithelia constitute the fundamental tissue barriers of metazoan organisms. Epithelial cells form sheets that line the surface of organs and are connected to each other by cell-cell adhesion molecules. These adhesion systems include E-cadherin, a transmembrane protein that mediates homophilic cell-cell adhesion to form cohesive cell-cell junctions (Niessen et al, 2011; Liang et al 2015; van Roy & Berx 2008). E-cadherin molecules distribute as clusters throughout the lateral surfaces where epithelial cells come into contact with one another (Wu Y, et al. 2015; Wu SK, et al. 2014a; Wu SK, et al. 2014b). In simple polarized epithelia, E-cadherin clusters also show distinct patterns of organization within cell-cell contacts. In the apical region of contacts, E-cadherin clusters concentrate in a relatively immobile ring-like structure to form the zonula adherens (ZA). In contrast, within the lateral junctions, located basal to the ZA, E-cadherin clusters undergo dynamic movements in the plane of the plasma membrane. These differences in cadherin motion reflect differences in the dynamic behavior of the junctional actomyosin cytoskeleton (Wu SK et al, 2014a, Moore et al, 2014).

At junctions, cadherins also mechanically couple the contractile cytoskeletons of neighbouring cells together, leading to the generation of junctional tension (Maître & Heisenberg 2013). This is reflected in the concentration of actomyosin at both the ZA and lateral cell-cell junctions. However, the cortical cytoskeleton at the ZA is able to generate strong, sustained contractile force, whereas stress-induced turnover of cortical actin leads to the dissipation of contractile stress at the lateral junctions (Wu SK, et al. 2014a). In consequence, junctional tension at the ZA (hereafter referred to as line tension) is greater than that at the lateral junctions. Junctional tension has been demonstrated experimentally in a variety of systems, from Drosophila and Zebrafish embryos to cultured cells (Hutson et al., 2003; Fernandez-Gonzalez et al., 2009; Ratheesh et al., 2012, Martin, 2010).

Epithelia must preserve their barrier integrity despite a range of challenges, including cell death, injury, infection and cell division (Gomez et al, 2011). In all these instances, cadherin junctions must reorganize without compromising tissue integrity. A noteworthy example here is the case of microscopic tissue injury and wounds (Sonnemann & Bement 2011). Microscopic wounds occur when small numbers of cells are damaged (e.g. one to five cells) and these wounds must be repaired for tissue integrity to be maintained. Time-lapse imaging has revealed that the area of microscopic wounds typically changes in a non-monotonic fashion, first opening and then closing (healing) over a period of 10 min to 1 hour. The healing of microscopic wounds may involve multiple mechanisms (Martin & Lewis, 1992, Brock et al., 1996, Buck, 1979, Sonnemann & Bement, 2011). One is the migration of cells from the edge of the wound into the injury space, a process that involves lamellipodial cell motility. A second mechanism entails the contraction of cells underlying the wound,

which occurs when epithelia overlay other tissues, such as the amnioserosa of the Drosophila embryo. Thirdly, the cells at the margins of wounds can form an actomyosin ring (purse-string) that encloses the wound. Contraction of the purse-string then pulls neighbouring cells into the wound to drive wound closure (Abreu-Blanco et al., 2012, Antunes et al., 2013). The relative importance and coordination of these mechanisms differs depending on the model system tested and its developmental context.

The Cellular Potts Model (CPM) developed by Glazier and Graner (1992, 1993) and its off-lattice alternative, the vertex model (Nagai & Honda, 2001, Nagai & Honda, 2009, Fletcher et al, 2014), are computational algorithms designed to represent cell organization at small scales (from a few to hundreds of cells); they are particularly suited to study the dynamics of such systems in the presence of microscopic wounds. However, a potentially significant difference between the two models lies in their representation of cell edges: the CPM allows for arbitrary, whereas, by definition, the vertex model utilizes straight cell edges, or in certain variants curved boundaries with constant curvature (Ishimoto & Morishita, 2014) We use the CPM to investigate microscopic wound repair and the interactions of adhesion and contraction that influence the repair process. Minimization of the energy of the CPM using simulation leads to either a *hard* regime or a *soft* regime, the boundary between these regimes depending on the relative contribution of adhesion and line tension to the energy function of the system. When applied to microscopic wounds, the interaction between contractile junctional tension and adhesion between the cells plays an important role in determining whether a site of damage will monotonically increase and stay open or whether it will close and heal. Moreover, our theoretical analysis predicts that in the *hard* regime, there is a critical wound size above which the wound will not close. Thus our data suggest that changing the balance between contraction and adhesion at the cell-cell junctions is required for non-monotonic wound closure to occur.

2 The Model and simulations of epithelial cell monolayers at steady state

We model the epithelial cell layer and micro-wounds in two dimensions using the CPM, which represents the apical region of cells, the sites where the zonulae adherente are located, as collections of pixels on a lattice (Szabo et al, 2010; Kabla, 2012). Depending on which cell it belongs to, each pixel is assigned a cell index j (represented by different colours in Fig. 1). The cells evolve in time by randomly selecting a pixel at the boundary between two cells, and measuring the change in an "energy" function ΔE that would result if the pixel were reassigned to a neighbouring cell. If the energy decreases ($\Delta E \leq 0$), the index change is always allowed, whereas if the energy increases, ($\Delta E > 0$), the site index change is allowed with the probability $exp\left(-\frac{\Delta E}{T}\right)$, where T is a temperature-like parameter that controls "noise" in the system. Each and every pixel is given the opportunity of an index change and this represents one Monte Carlo Step (MCS), which we refer to as a single iteration in the CPM. Changing the cell index of the pixels at the boundaries between neighbouring cells allows the cell boundaries to change.

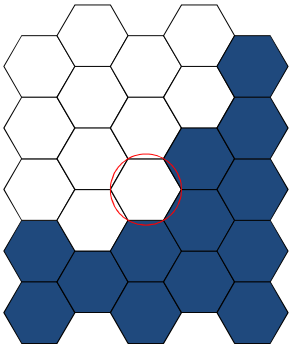

Figure 1 Representation of cells as groups of pixels on a hexagonal lattice where pixels change their labels to one of their neighbours. The hexagons of a given colour represent pixels belonging to different cells.

To prevent the biologically unrealistic situation in which the simulated cells may increase their perimeter by breaking up into multiple disconnected regions, we add an additional constraint in the model that explicitly restricts pixel changes to configurations where every cell is represented by singly connected domain of pixels.

The dynamics of the model are driven by minimizing a phenomenological energy determined by cell configurations. We use the same form of the energy function that has been previously used in models of cell-cell interactions (Farhadifar et al, 2007). In particular, the Vertex model (Farhadifar et al, 2007) is based on a simplified representation of cells as polygons; their shape is determined by tracking the

movement of cell vertices. The total energy of a system of *N*-cells is defined in terms of the area A_j and perimeter L_j of *j*th cell through the sum

$$E(A_j, L_j) = \frac{k}{2}\sum_{j}^{N}(A_j - A_p)^2 + \frac{\Gamma}{2}\sum_{j}^{N} {L_j}^2 - \frac{S}{2}\sum_{j}^{N} L_j$$

The first term represents an energy cost for deviating from a preferred area A_p, i.e. the cells resist expansion or compression. The second term models the contractile line tension due to the apical actin ring around the perimeter of the cells, while the last term represents cell-to-cell adhesion, attributed to the presence of adhesion molecules like E-cadherin, and is proportional to the perimeter of the cells. The parameters k, Γ and S determine the relative magnitude of the different contributions to the energy.

Note, that the adhesion term is assumed to be negative, i.e. the cells preferentially expand their boundaries shared with neigbouring cells, however, this competes with the contractile tension that dominates when the perimeter becomes elongated. For the pixel based CPM the adhesion interaction term is commonly expressed using the double sum

$$\sum_{i,j}^{N}(1 - \delta_{\sigma(i),\sigma(j)})$$

where σ are the site labels and the Kronecker delta term prevents counting contributions to the energy from pixels that belong to the same cell. This term counts the number of pixels on the edges of the cells and we used this to compute the perimeter L_j.

In order to eliminate "internal pressure" in the system we assume that the preferred cell area, A_p, coincides with the total area of the simulation domain divided by the number of cells $A_p = A_T/N$, so that the cell layer is not compressed or stretched.

2.1 **Hard and soft regime**

First, we consider the steady state condition of a confluent monolayer of cells. We performed numerical simulations of the CPM and characterized the morphology and dynamical behavior of cells in the stationary state. We found that the cell shape is primarily determined by the interaction between contraction (the second term in the energy formula) and adhesion (third term in the energy).

For high contractility values, cells exhibit straight contacts and polygonal shape with a typical vertex number of 6. In contrast, when the adhesion term dominates, cells lose their regular pattern of organization and cell contacts become more irregular and wavy. Examples of the model showing the two regimes are given in Fig. 2 (see also Supplementary Movies 1a-d). It has been shown that when contractility is inhibited, either by direct perturbation of the actin cytoskeleton (Caldwell et al, 2014, Kovacs et al, 2011) or by disrupting the signaling pathways that regulate actomyosin (Otani et al, 2006, Gomez et al, 2015), cells exhibit these properties of junctional organization, showing a good concordance with the results of our CPM model.

The above-mentioned behavior is similar to that of the vertex model with the same energy function that was described in Farhadifar et al (2007). Differences between the two models arise, however, due to the different representation of the cell boundaries in the two models. The CPM allows for non-polygonal boundaries leading to the formation of irregular cell protrusions in the soft regime.

To better study the role of model parameters and the transition between the hard (high contractility) and soft (low contractility) regimes of junctional organization it is useful to theoretically analyze the model. The effect of competition between contractility (shortening) and adhesion (elongating) on the cell perimeter is best seen by combining the quadratic and linear terms of the cell perimeter and completing the square to give:

$$E(A_j, L_j) = \frac{\mathrm{k}}{2}\sum_{j}^{N}(A_j - A_p)^2 + \frac{\Gamma}{2}\sum_{j}^{N}(L_j - L_p)^2 + \frac{\Gamma N}{2}{L_p}^2$$

where

$$L_p = S/2\Gamma.$$

The constant term $\frac{\Gamma N}{2}{L_p}^2$ can be neglected as it does not influence the behavior of the system. This form of the energy function shows that, in addition to the preferred cell area, A_p, the cells also have a preferred cell perimeter, L_p, whose value is not prescribed, but arises from the competition between cell-to-cell adhesion and contractile line tension.

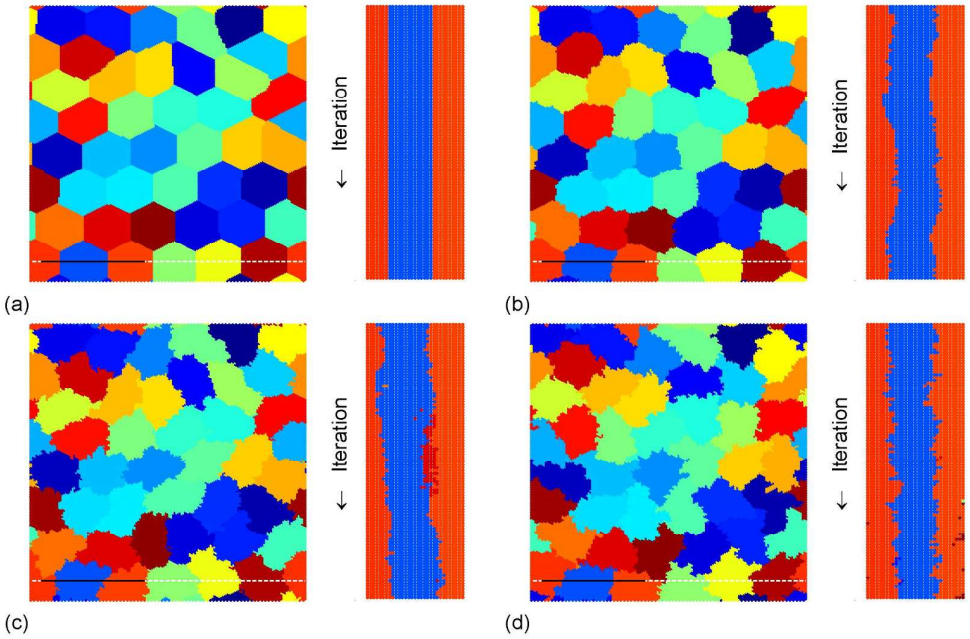

Figure 3: Distribution of the cells in the different regimes and kymographs showing the time evolution of cell junctions (at the location indicated by the black line); (a) represents a very hard system of cells creating quasi-polygonal shapes close to a hexagon, $S = 1500$ and $\Gamma = 6$ at $T = 10$; (b) the cells are still in a hard regime, but with a higher temperature $S = 1500$ and $\Gamma = 6$ at $T = 500$; (c) example of cells in the soft regime, $S = 3000$ and $\Gamma = 6$ at low temperature $T = 10$; (d) soft regime at higher temperature, $S = 3000$ and $\Gamma = 6$ at $T = 500$. All simulations use parameters $k = 2$ and $N = 44$ on a 160×160 hexagonal pixel grid.

Depending on the geometry of the cells, the average/preferred cell area may correspond to different values of the cell perimeter length. Although the energy function stipulates a preferred perimeter, it has an upper and lower bound for a fixed cell area comprised of finite pixels. The upper bound corresponds to a long cell of single pixel width, and is less relevant for cell modelling. More interesting is the lower bound, defined by the shortest boundary that can enclose a cell of given area. In a single cell problem this would be the circumference of a circle, in a regular tiling the *Honeycomb conjecture* (proven by T. Hales, 2001) states that the minimum perimeter is given by that of a hexagon. The number of pixels along the perimeter of a hexagonal cell made up of hexagonal pixels is (Figure 3)

$$L_n = 12n - 6$$

where n is the number of pixel layers making up the cell, and the area of the hexagonal cell is

$$A_n = 3n^2 - 3n + 1$$

We use this to calculate an approximation for the minimal perimeter

$$L_{min} = 2\sqrt{12A_p - 3}$$

The model depends strongly on whether the preferred cell perimeter, L_p is larger or smaller than L_{min} leading to a *hard* and the *soft* regime with qualitatively different behaviour.

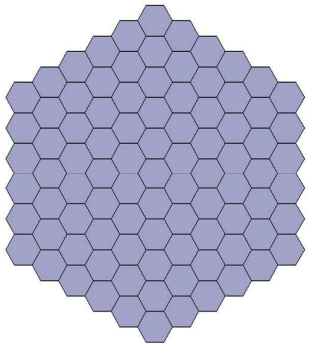

Figure 3 Representation of a hexagonal cell created with $n = 6$ hexagonal pixel layers.

In the *hard* regime, the cells cannot reach their preferred perimeter, L_p, since $L_p < L_{min}$. So their perimeter is close to the minimum perimeter. In this case the energy minimum corresponds to the hexagonal tiling and contraction along the perimeters dominates, creating a tight configuration with mechanical tension maintained along the cell interfaces. Numerical simulations, with a relatively small temperature parameter, are consistent with a quasi-hexagonal tiling with fluctuations arising from defects along cell boundaries (Fig 2a).

In the alternate case, where $L_p > L_{min}$, we have a *soft* regime. Cell boundaries are loose and become more wavy. The energy minimum is highly degenerate, i.e. there are infinitely many possible spatial configurations that satisfy both the area and perimeter constraints. The consequence of this degeneracy is that the junctions are very irregular (non-linear) in shape and mobile, even at low temperatures (Figure 2c,d).

This interpretation is confirmed by computing the average cell perimeter attained by the cells (Fig. 4a, b). In the *hard* regime this is approximately equal to L_{min} whereas in the *soft* regime the average cell perimeter is approximately L_p. Of note, the temperature in the system also plays a role in determining the cell shape in the model. In the hard regime increasing the temperature causes the cells to change from regular hexagons to more irregular cell shapes (Fig 2b).

Finally, we analyzed the dynamics of cell-cell boundaries in the hard and soft regimes (Fig 4c). We found that the number of pixel changes per iteration is approximately constant in the *hard* regime. In contrast, as the simulations move to the "soft" regime the number of pixel changes increases with L_p, implying that cell boundaries in the soft regime are more dynamic than in the hard regime. Earlier, we found experimentally that contractile tension at the ZA is greater than that at the lateral junctions (Wu SK, et al 2014). A prediction of our model analysis is that these differences in tension will lead to differences in the dynamics of these regions. To test this, we performed live cell imaging of cell-cell junctions at the apical and lateral junctions of cells. We found that, in qualitative agreement with the simulations, cell-cell boundaries at the lateral junctions are more curved and dynamic than those at the corresponding apical junctions (Fig. 5, Supplementary Movie 2). This further suggests that the balance between adhesion and contractility not only determines the amount of tension at the cell-cell junctions but also influences the plasticity of the cell-cell interface.

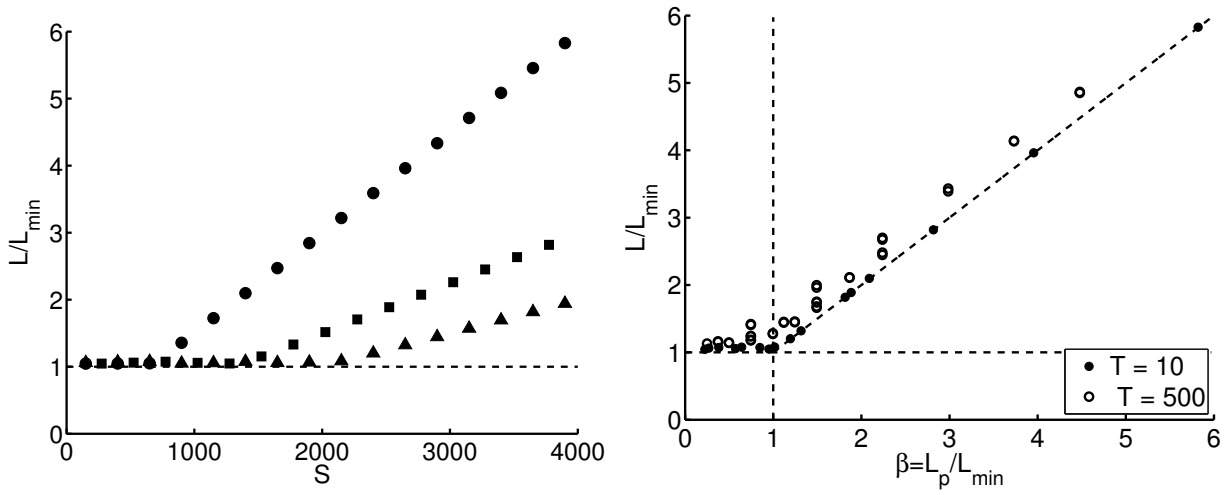

(a) (b)

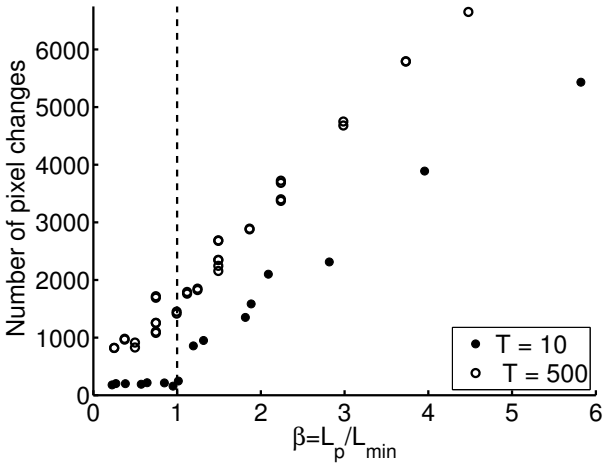

(c)

Figure 4: Representation of the change from the *hard* to *soft* regime; (a) average perimeter of the cells as a function of the adhesion coefficient S. The symbols represent simulations for different values of the line tension parameter Γ ($\Gamma = 2$, circles $\Gamma = 4$ squares, and $\Gamma = 6$ triangles). (b) rescaling the adhesion coefficient on the horizontal axis ($L_p = S/2\Gamma$) shows the comparison between cell perimeters and the preferred perimeter L_p. The perimeter is approximately constant in the *hard* regime (L_p/L_{min} <1) but increases linearly in the soft regime (L_p/L_{min} > 1). (c) shows the number of pixel changes that occur in a single iteration. In the *hard* regime the cells have a fairly constant number of changes but that increases when the cells move into the *soft* regime. The other parameters are $k = 2$ and $N = 44$ on a 160×160 hexagonal pixel grid.

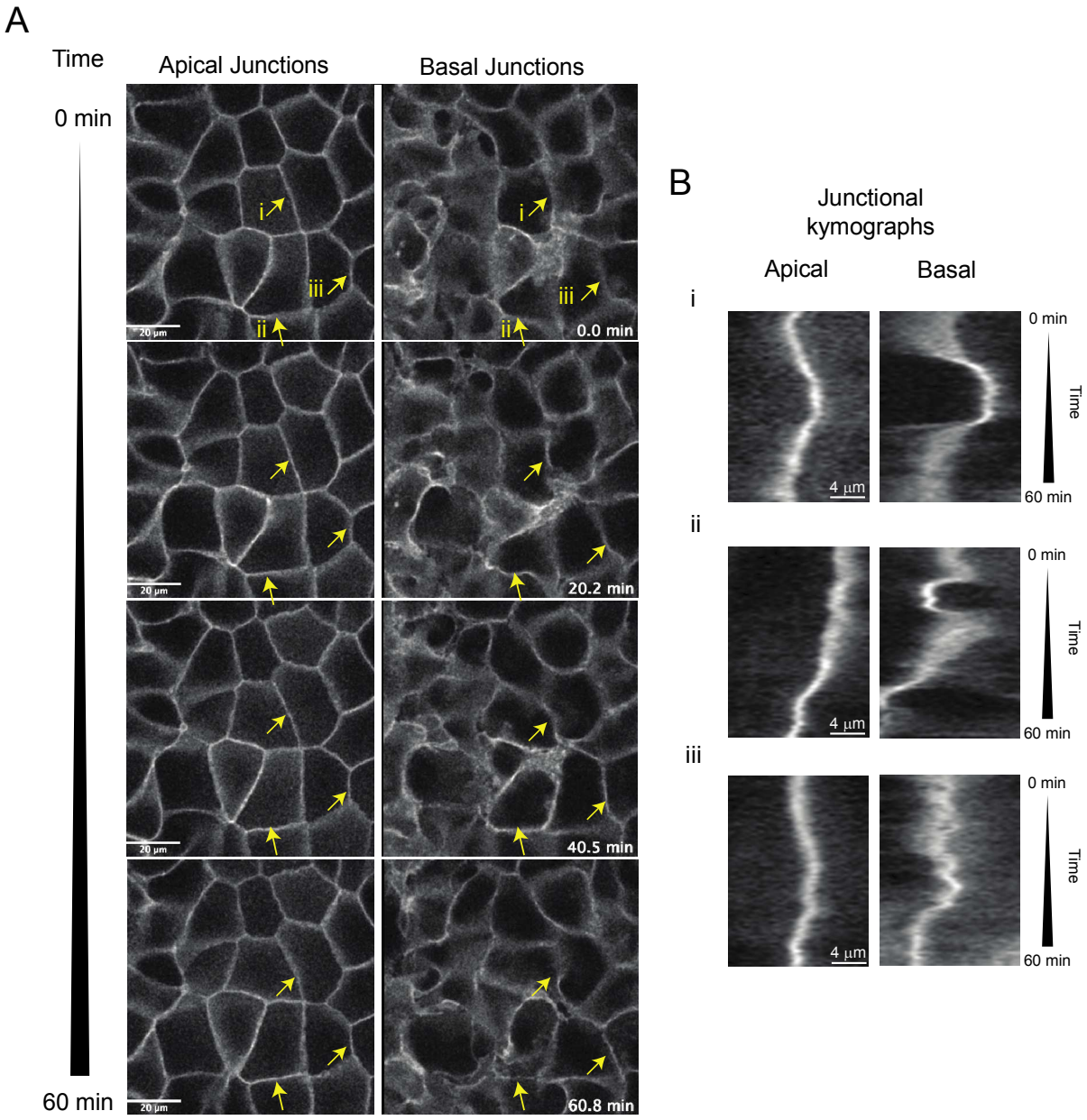

Figure. 5. Morphology of apical (ZA) and lateral cell-cell contacts within confluent epithelial cells. (a) Cells expressing a plasma membrane targeted fluorescent reporter were imaged by confocal live cell microscopy. Images taken at various times during the movie are shown (times indicated in far right of each panel). Left and right panels correspond to different Z positions, one located to the top of the cells (apical junctions, left) and the other 4 µm below in the basal direction (basal junctions, right). Scale bar=20 µm. (b) Kymographs showing the time evolution of the apical and basal cell junctions indicated by the arrows on the left panel.

3 Simulations of the system in the presence of a microscopic injury or wound

Now we consider the dynamic behaviour of the system in response to a small injury or wound, so that M adjacent cells are eliminated. In the model we remove the terms corresponding to the injured cells from the energy equation. Removal of these cells also affects the adhesion along the interface between the normal cells and the injury site. Accordingly, the adhesion term is now composed of two parts, one where a cell is connected to other neighbouring cells and the other where the cell is adjacent to a cell that is being removed and where there is no adhesion contribution to the energy. Thus, after completing the square in the energy function and grouping the terms corresponding to the cell boundaries along the injury, we obtain a new adhesion term that is proportional to the injury perimeter L_w

$$E(A_j, L_j, L_w) = \frac{\mathrm{k}}{2}\sum_{j}^{N-M}\left(A_j - A_p\right)^2 + \frac{\Gamma}{2}\sum_{j}^{N-M}\left(L_j - L_p\right)^2 + SL_w + \frac{\Gamma\,(N-M){L_p}^2}{2}$$

Note, however, that the new positive adhesion term, which arises as a consequence of the wound, represents an empty space within the sheet, denoting the absence of adhesion along its perimeter.

If, after removing cells, the wound perimeter reaches zero, it implies that the system has evolved to a state where the wound closes completely. Reducing L_w has competing energy costs involving the extension of cell area on the cells surrounding the wound and, in the *hard* regime, also requires an increase in their cell perimeter.

Thus, we performed numerical simulations where first we let the system to reach equilibrium before the wound was created. The simulations for different parameters show that the area of the injury can expand from its original value then reach a fluctuating steady state, or decrease to a smaller area and eventually close completely. These cases can be seen in Figure 6 (see also Supplementary Movies 3a,b). In all cases the change is monotonic in time. In general the equilibrium wound size is determined by the competition between adhesion and apical contractile (line) tension. When the perimeter contraction coefficient Γ is kept constant the equilibrium wound size decreases as the adhesion coefficient is increased. Moreover, the wound closes spontaneously when the adhesion coefficient is larger than a certain threshold. This threshold in the adhesion parameter decreases when the contraction coefficient is reduced. Qualitatively, spontaneous wound closure occurs with weak perimeter contraction and/or strong adhesion, i.e. when the system is approaching the *soft* regime, a result that has been also suggested during the extrusion of dying cells (Kuipers D et al, 2014).

Although the wound closure in the model is primarily determined by adhesion and contraction we found that the temperature parameter T can also have some effect on the results of the simulations. When the temperature is too low the wound may not open or close to the equilibrium wound size that would be reached with higher values of *T*. This is because the system is unable to move easily between different states to reach the optimal configuration. This means that the noise amplitude must be taken into consideration, as it has to be large enough to change the system configuration but small enough to maintain realistic cell shapes over cellular time scales.

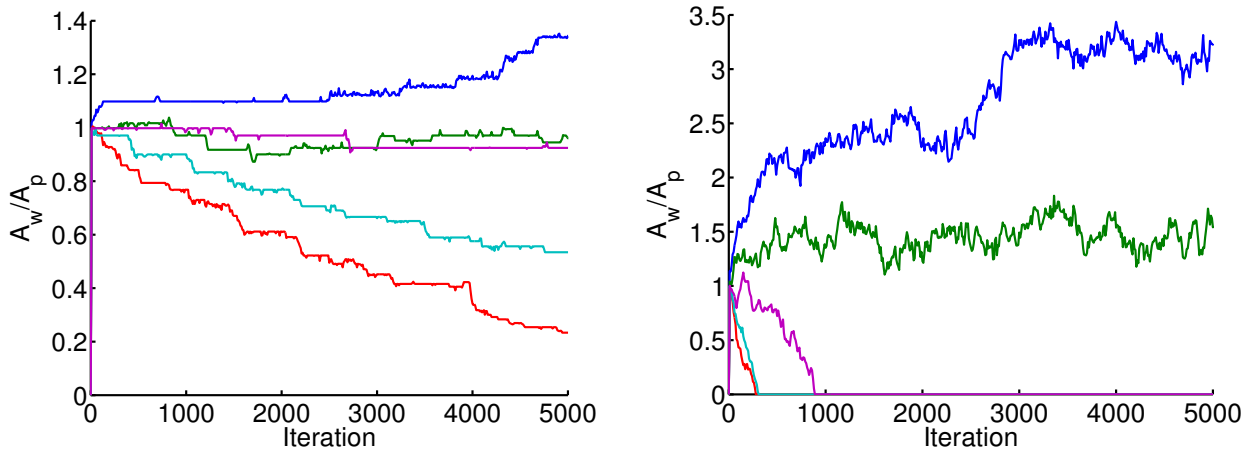

(a) (b)

Figure 6: Injury size vs "time" (iteration) showing how the initial injury may expand or collapse given different parameters for two different temperatures (a) $T = 100$ and (b) $T = 500$. Each line represents a different combination of Γ and S, blue $\Gamma = 6$ and $S = 700$, green $\Gamma = 4$ and $S = 700$, red $\Gamma = 4$ and $S = 900$, cyan $\Gamma = 6$ and $S = 1500$ and magenta $\Gamma = 6$ and $S = 1500$. All simulation have other parameters as $k = 2$ and $N = 44$ on a 160×160 hexagonal pixel grid.

4 Equilibrium injury size

In order to better understand the mechanism that determines the closure threshold and the dependence of equilibrium wound area on the parameters of the model, we make several simplifying assumptions to rewrite the energy of the system as a function of a single variable, the wound perimeter, and then determine the energy minima corresponding to the equilibrium state. First, we assume that the area and perimeter of the cells are all identical: $A_j = A_c$ and $L_j = L_c$ for $j = 1, \dots, N$ so the energy becomes

$$E(A_j, L_j, L_w) = \frac{\mathrm{k(N-M)}}{2}(A_c - A_p)^2 + \frac{\Gamma(\mathrm{N-M})}{2}(L_c - L_p)^2 + SL_w$$

Conservation of area links the wound area to the cell area A_c and total area $A_T = NA_p$ through the relation

$$A_w + (N - M)A_c = A_T$$

To proceed, we need to estimate the relationship between the area of the cells and their perimeter. This relationship depends on the shape of the cells but in general can be written in the form $A_c = gL_c^2$. For example, for a true hexagonal shape $g = 1/4\sqrt{3}$ or for a circle $g = 1/4\pi$. For the hexagonal cell made of n hexagonal pixel layers,

$$g^* = \frac{3n^2 - 3n + 1}{(12n - 6)^2} = \frac{1}{48} + \frac{1}{4(12n - 6)^2}$$

So for $n >> 1$ $g^* \approx 1/48$.

For simplicity we assume that the shape parameter of the wound and cells are approximately the same so $A_w = g\,{L_w}^2$. Using the area conservation

$$A_c = \frac{1}{N - M}(NA_p - A_w)$$

the relationship between the linear dimensions of the wound and cells can be written as

$$L_c = \sqrt{\frac{NA_p}{g(N - M)} - \frac{{L_w}^2}{N - M}}$$

Essentially this states that reduction in the wound perimeter, leads to a reduction in the wound area, the excess area is then equally shared among the live cells so that their perimeter grows (and vice versa for an increase in the wound perimeter). This allows us now to eliminate the live cell perimeter from the energy and write it as a function of the wound perimeter alone

$$E(L_w) = \frac{k}{2(N-M)}\left(MA_p - g{L_w}^2\right)^2 + \frac{\Gamma A_p}{2g}\left(\sqrt{\frac{NA_p}{g} - {L_w}^2} - L_p\sqrt{N-M}\right)^2 + \frac{S}{2}L_w,$$

By using as length scale unit the cell perimeter corresponding to the preferred area A_p we introduce the non-dimensional variable $l_w = L_w\sqrt{g/A_p}$ and the non-dimensional control parameter $\beta = L_p\sqrt{g/A_p} = S\sqrt{g}/(2\Gamma\sqrt{A_p})$ the energy function becomes

$$E^*(l_w) = \frac{2E}{S}\sqrt{\frac{g}{A_p}} = \frac{\phi M^2}{(N-M)}\left(1 - \frac{{l_w}^2}{M}\right)^2 + \frac{1}{2\beta}\left(\sqrt{N - {l_w}^2} - \beta\sqrt{N-M}\right)^2 + l_w$$

where $\phi = k g^{1/2} {A_p}^{3/2}/S$. The equilibrium states of the system are represented by the minima of the energy function. We find that there are two cases. In the first case there are two minima: one corresponding to positive values of the wound perimeter l_w and the other one to negative (unphysical) values. In the other case there is only one energy minimum for negative values of l_w. Figure 7 shows the two cases.

In the first case (identified by the dashed line in Fig 7) the two minima are separated by a local maximum. If the initial wound size, l_w, is larger than the local maximum the wound will open to the local minimum. Alternatively if the value of the initial wound size is lower than the maximum, then the wound will close to $l_w = 0$. In the second case, no positive equilibrium solutions exist so the wound will always close from any initial size. The transition from case 1 to case 2 occurs when the control parameter β is increased, i.e. the balance between adhesion versus apical line tension is modified in the favor of adhesion. In this case the energy minimum attains the same value as the maximum and disappears, leaving no equilibrium state with positive l_w, which indicates that the wound dimension decreases to zero. Physically the cells are driven by adhesion to "zip up" the wound, as the contractile resistance is insufficient to exert a countervailing force.

The values for the equilibrium wound size are obtained by finding the wound length(s) that satisfies

$$\frac{dE^*(l_w)}{dl_w} = \frac{4\phi {l_w}^3}{N-M} - \left(\frac{4\phi M}{N-M} + \frac{1}{\beta}\right)l_w + \frac{l_w\sqrt{1-\frac{M}{N}}}{\sqrt{1-\frac{{l_w}^2}{N}}} + 1 = 0.$$

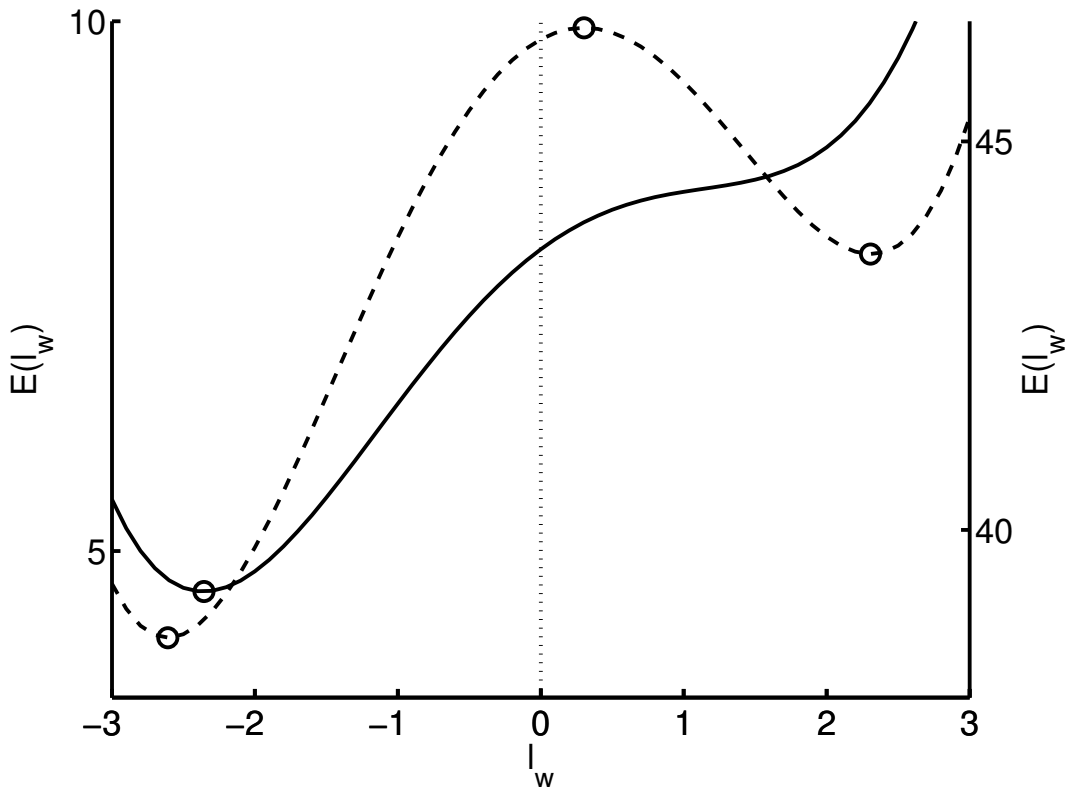

Figure 7: Plot of the energy function $E(l_w)$ with parameters $S = 700$ and $\Gamma = 8$ (dashed line, right axis) and $S = 1500$ and $\Gamma = 8$ (solid line, left axis). Other parameters are $k = 2$, $N = 44$, $M = 1$ and $g = 1/48$

A slightly simplified form of the equation for the energy derivative function can be obtained by using the assumption that N >> 1 and using Taylor expansion (in $1/N$) we obtain the equation

$$\frac{dE^*(l_w)}{dl_w} = -\left(\frac{4\phi}{N-M} + \frac{1}{2N}\right) {l_w}^3 + \left(\frac{4\phi M}{N-M} + \frac{1}{\beta} - 1\right) l_w - 1 = 0 \Bigg]_{N \gg 1}$$

Thus the equilibrium wound size corresponds to the positive root of a cubic equation of the form

$$-a{l_w}^3 + bl_w - 1 = 0$$

where $a > 0$ for any parameter combination. So if $b < 0$ no positive roots exist, i.e. the wound will always close. We let $\varepsilon = \frac{4\phi M}{N-M}$, that is a small positive number for $N \gg M$. Thus a sufficient condition for wound closure is

$$\frac{L_{min}}{L_p} < 1 - \varepsilon = 1 - \frac{4k g^{1/2} {A_p}^{2/3} M}{S(N-M)}.$$

This suggests that the wound in the simulations with cells in the *soft* regime, $\frac{L_{min}}{L_p} < 1$, will always close if N is sufficiently large.

Using the above expression for the energy as a function of wound size we can determine numerically the positive roots of the energy derivative function: $\frac{dE^*(l_w)}{dl_w} = 0$. Comparing these with results from the full numerical simulations of the CPM (Figure 8), we obtain a reasonable approximation of the equilibrium wound size and of the transition to possible wound closure when the parameters S and Γ are varied. For example, for the particular case of $\Gamma = 2$, $S = 200$ and an initial wound $l_w = 1$, the system corresponds to a *hard* regime in which the wound will open and reach an equilibrium value of around ~1.2 (blue solid line). However, if the initial wound size is lower than l_w= ~0.2 (blue dashed line), then the wound will start to collapse and eventually close. Thus, whether or not the wound size l_w is larger or smaller than the location of the energy maximum, which corresponds to an unstable wound solution, will determine whether or not the wound will close or open. In addition, if we keep constant all the parameters but increase the adhesion coefficient S, the local maximum corresponding to l_w disappears, implying that the wound will close independently of its initial size.

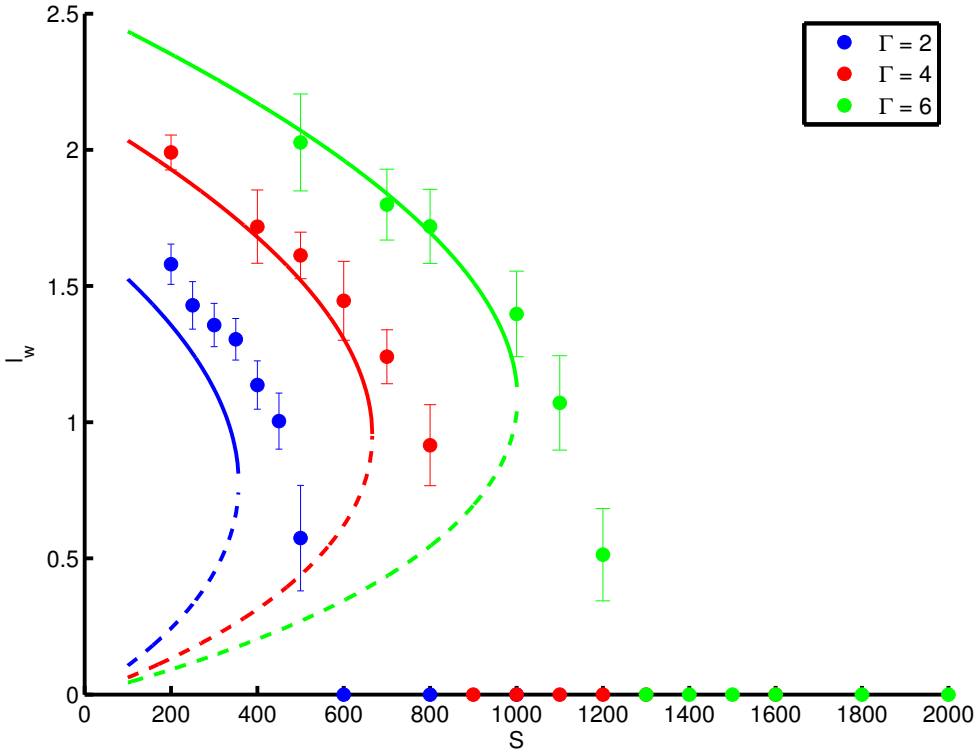

Figure 8: Comparison of the theoretical approximation of equilibrium with the direct numerical results from the CPM simulations: showing the normalized wound area as a function of the adhesion coefficient S for different values of the line tension parameter Γ. The solid line represents the local energy minimum and the dashed line is the local energy maximum. Other parameters are $k = 2$ and $N = 44$ on a 160×160 grid of hexagonal pixels with one cell removed, $M = 1$.

We then used this theoretical approach to the equilibrium wound size and closure threshold to investigate the dependence on the number of cells *N*. Varying the control parameter $\beta = \frac{L_p}{L_{min}}$, that changes the relative strength of adhesion vs. contraction, we found that the threshold for spontaneous wound closure from any initial size (i.e. when the open equilibrium wound state disappears) shifts towards higher adhesion values as *N* is increased (Figure 9a) and approaches the boundary between the *hard* and *soft* regime $\beta = 1$ for large *N*. The equilibrium wound size also increases with the number of cells as $l_w \sim \sqrt{N}$ (Figure 9b). This is because in the hard regime the cells contract their perimeter when a wound is created, which is then balanced by the increase of wound perimeter. Since the contractile tension term in the energy function is proportional to the number of cells, the equilibrium is reached for a larger wound size as the cell number increases. However, in real tissues, it is likely that the number of cells affected by the mechanical perturbation due to injury is limited to a finite neighbourhood of the wound (e.g. due to adhesion to underlying tissue), which was not taken into account in our theoretical analysis.

In addition to relaxing the tension in the tissue, by increased adhesion or reduced perimeter contraction, other mechanisms can also contribute to the process of wound closure. An example of this is the formation of a supra-cellular purse string that contracts the perimeter of the wound (Vedula et al, 2015). This mechanism can be easily included in the energy function as an extra term similar to the cell perimeter contraction term,

$$+\frac{\Gamma^*}{2}{L_w}^2,$$

with a contraction strength of Γ^*. We can then use our theoretical approximation to determine the equilibrium wound size from the positive root of the energy derivative function. As expected, increasing the strength of the purse string, Γ^*, the wound closure threshold shifts further into the *hard* regime meaning that wound closure could be favorable even for a system in the hard regime (Figure 10).

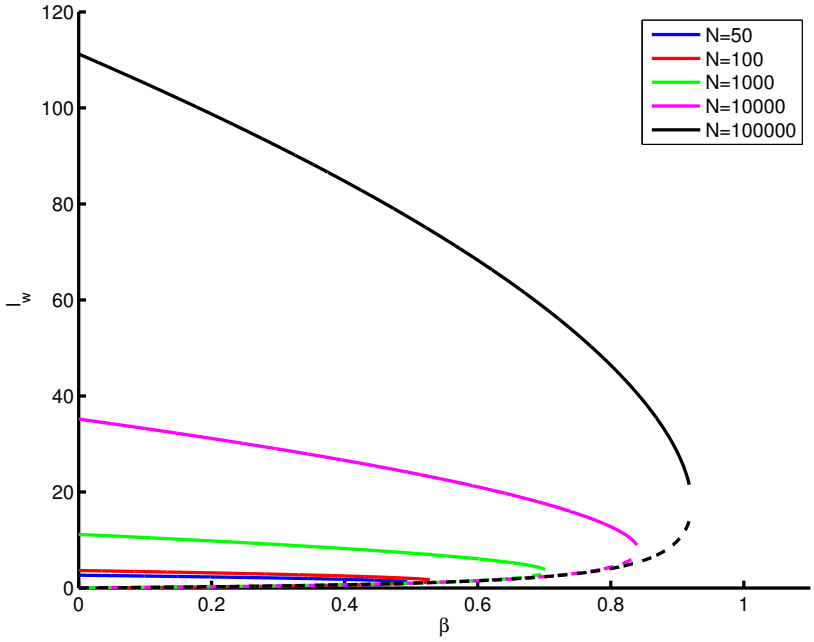

(a)

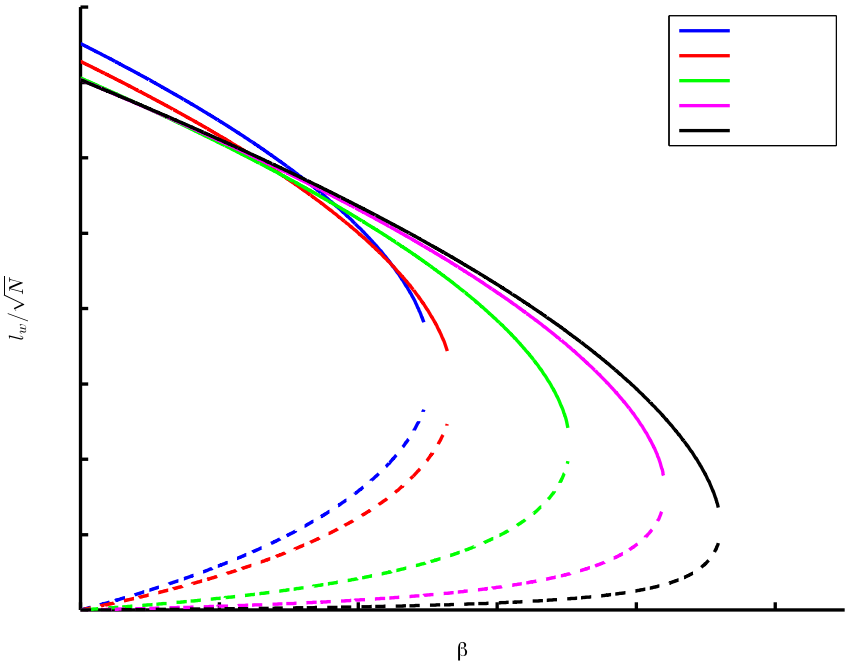

(b)

Figure 9: Equilibrium wound size obtained from the theoretical approximation: (a) *stable* equilibrium wound size (solid line) and *unstable* equilibrium wound size (dashed line) against $\beta = L_p/L_{min}$. The parameters are $\Gamma = 6$, $k = 2$, $A_0 = 582$ with one cell removed, $M = 1$, for different number of cells in the system $N = (50,100,1000,10000,100000)$; (b) same as (a) but the wound size, vertical axis, is rescaled as $l_w/\sqrt{N}$.

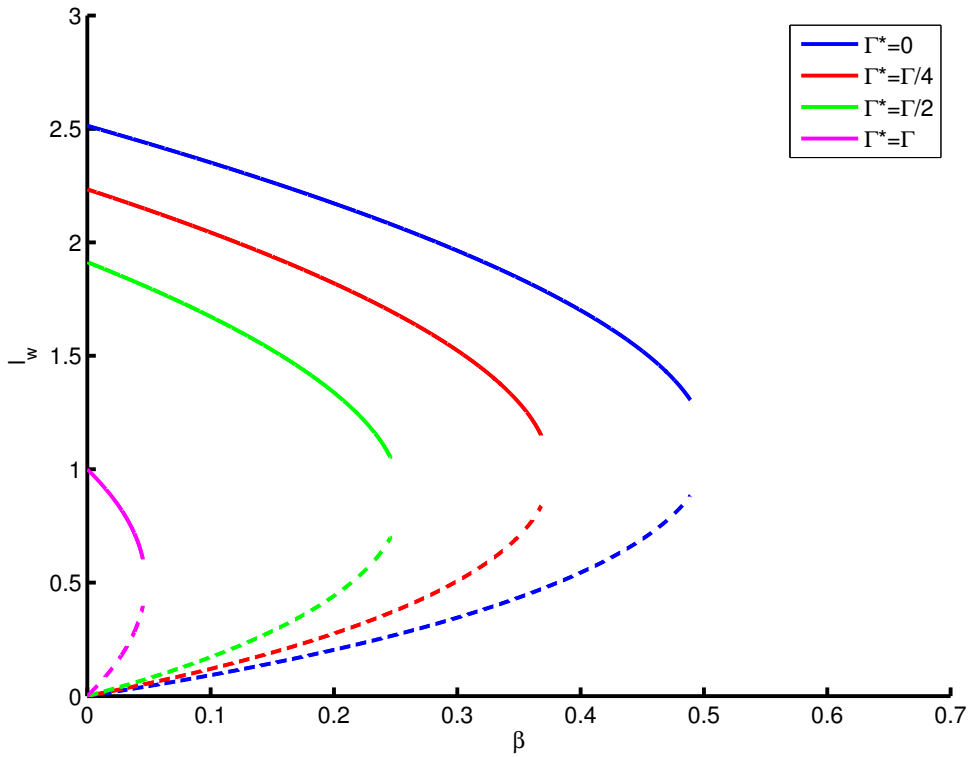

Figure 10: Equilibrium wound size calculated from the theoretical approximation, with the addition of the contractile purse string around the wound. Stable equilibrium wound size (solid line) and unstable equilibrium wound size (dashed line) against $\beta = L_p/L_{min}$. The parameters are $\Gamma = 6$, $k = 2$, $A_0 = 582$ and $N = 44$ with one cell removed, $M = 1$, for different strengths of the contraction of the wound perimeter $\Gamma^* = (0, \Gamma/4, \Gamma/2, \Gamma)$.

5 Discussion

We have used the CPM to describe an epithelium including simple mechanical representations of adhesion, contraction and pressure in the cells (Graner & Glazier, 1992; Szabo et al, 2010, Kabla, 2012). Using these components we can find two regimes where the cells can sit, either in a hard regime where cell shape is governed by the contractile line tension or in a soft regime, where the cell shape is determined by adhesion. This is similar to what has been described using a vertex model (Farhadifar et al, 2007). However, by implementing a CPM model we were able to obtain a more accurate representation of cell shapes when compared with the vertex model, particularly of the cell shapes that correspond to a soft regime. Additionally, our CPM model also allowed us to characterize more precisely

the dynamics of cell boundaries, yielding simulations that are in agreement with previous experimental observations. In particular, we found that for steady state conditions apical junctions of cells exhibit properties that are well characterized by a hard regime in the model. Altogether, this offers an advantage of the CPM approach compared to the vertex models.

Using this cell representation and adding a microscopic wound in it, we observe that the wound can increase (open) or decrease (close) its area depending on the relative balance between adhesion and line tension. Experimental data indicate that performing a micro wound by laser irradiation leads to a rapid relaxation of the perimeter of the injured area (Antunes M et al, 2013; Fernandez-Gonzalez, 2013) followed by the reorganization of the junction around the injury. Combined with our theoretical analysis, these observations imply that for a wound to close it is necessary for the properties of the cells to change to favour the remodeling of the junctional organization around the wound. Evidence in the literature suggests that the response of cells to the wounding process is complex and may involve different complementary and overlapping mechanisms that involve biochemical or mechanical signals (Antunes M et al, 2013; Fernandez-Gonzalez, 2013; Brugués et al, 2014; Abreu-Blanco; Anon et al, 2012; Tamada et al, 2007). For example it has been described that calcium waves around the wound site are able to propagate waves of myosin activation (contractility) that alter the morphology of the cells surrounding the wound, ultimately leading to the formation of a contractile purse string (Antunes et al, 2013). On the other hand, we have shown that myosin II is required for cadherin accumulation at the ZA (Smutny at al, 2010, Shewan et al, 2005), which suggests that myosin can influence cell-cell adhesion as well as contributing to line tension in junctions. Another factor that may influence wound closure is lamellipodial motility, which allows cells bordering a wound to migrate into, and thereby close, the wound (Abreu-Blanco et al, 2011; Anon et al, 2012). Cadherin adhesion is also required for the development of higher and polarized traction forces within epithelial sheets (Mertz, 2013, Weber, 2012). However, whether lamellipodial migration is coordinated or influenced by changes in cell-cell adhesion during wound healing is yet to be determined. Potentially, the complex interplay between these mechanisms may alter the properties of the cells surrounding a wound to ultimately favor the wound closure process.

Our theoretical analysis allowed us to estimate the equilibrium wound size using some assumptions. We found that when adhesion is weaker than a critical value (or equivalently

apical tension is above a certain threshold) an open wound represents the equilibrium state. However, the basin of attraction of the equilibrium state is limited by a minimum wound size (corresponding to the energy maximum) and wounds below this threshold close spontaneously. This can have several biological implications, particularly for microscopic defects in the monolayer on the scale of single cells. An interesting example occurs when individual cells undergo apoptosis within confluent epithelia. Under these conditions, the apoptotic cell contracts and reduces its apical area to eventually be extruded from the monolayer. Contraction of the dying cell (Kuipers et al, 2014, Brugues 2014, Monier B. et al, 2015) alters the shapes of its neighbouring cells, as the neighbours are pulled by the dying cell through cadherin-based cell-cell adhesion (Lubkov & Bar-Sagi, 2014; Grieve & Rabouille, 2014). Thus, the active contraction of the dying cell could be required to reduce its apical area below a minimal threshold, allowing neighbouring cells to spontaneously heal the monolayer at the same time dying cells are being extruded.

Similarly, the threshold in the wound size may have some relation to the purse-string mechanism of wound closure in small wounds, where an actomyosin contractile ring is formed in the cells that border the wound (Antunes et al, 2013, Abreu-Blanco et al, 2011, Fernandez-Gonzalez 2013). In this case the purse string contracts, thus reducing the wound size below the threshold that would allow it to close spontaneously even if an open wound equilibrium solution exists. However, for larger wounds, it is anticipated that higher forces could be required for this process to occur, which indeed can be facilitated if surrounding cells actively participate in the healing process as has been suggested recently (Kuipers et al, 2014).

Our results thus indicate that for the above-mentioned cases, either a change in contractility that helps to reduce the area size of the wound or an increase in adhesion (or reduction in tension) will favor spontaneous wound closure regardless of the initial size of the wound. Moreover, as cells at steady state behave like those in a hard regime, our modeling data also propose that for wounds which are larger than few cells, changes in the balance between contraction and adhesion is required for non-monotonous wound closure to occur. In particular, the properties of apical junctions of cells needs to be modified, in order to facilitate the remodeling required for efficient wound closure.

Supplementary material

Movie 1a-d: Simulation of different cell regimes; (a) system of cells creating quasi-polygonal shapes close to hexagons in the hard regime, $S = 500$ and $\Gamma = 6$ at $T = 500$; (b) close to the boundary between the hard and soft regimes, $S = 1500$ and $\Gamma = 6$ at $T = 500$; (c) example of cells in the soft regime, $S = 3000$ and $\Gamma = 6$ and $T = 100$; (d) far from the threshold in the soft regime showing elongated tendrils developing, $S = 5000$ and $\Gamma = 6$ at $T = 100$. Other simulations parameters are $k = 2$ and $N = 44$ on a 160×160 hexagonal pixel grid.

Movie 2: Live Cell Confocal microscopy of MCF-7 cells stably expressing a plasma membrane targeted fluorescent reporter. Time-lapse images were acquired as 12 z-stacks (0.8 μm z-step) and with an interval of 48.5 sec. Left and right corresponds to different Z positions, one located to the top of the cells (apical junctions, left) and the other 4 μm below in the basal direction (basal junctions, right). Scale bar=20 μm.

Movie 3a-b: Simulation of (a) an opening wound with parameters $S = 700$ and $\Gamma = 6$ and (b) a closing wound with parameters $S = 1300$ and $\Gamma = 6$. Other parameters: $k = 2$, $T = 500$ and $N = 44$ on a 160×160 hexagonal pixel grid

Experimental Procedures.

MCF-7 cells stably expressing a plasma membrane targeted fluorescent reporter, KRas-Src biosensor cloned into pCDNA3.1 (Seong et al, 2009), were obtained by transient transfection and antibiotic selection with G418 (Sigma) at 400 ug/ml. Resistant clones were isolated by fluorescence activated cell sorting (FACS).

Live Cell Confocal microscopy was performed on cells cultured on glass bottom dishes (Shengyou Biotechnology) at 37 C in a LSM 710 Zeiss microscope equipped with a ×63 oil immersion objective (Plan Apochromat ×40 1.3 NA, Zeiss). Fluorescence acquisition was performed using a 514 nm laser line for excitation and a 530-560 nm band pass for emission and time-lapse images were acquired as 12 z-stacks (0.8 μm z-step) and with an interval of 48.5 sec.

Acknowledgements

This work is supported by grants (1067405, 1037320) and a research fellowship (1044041) from the National Health and Medical Research Council of Australia; the Kids Cancer Project of the Oncology Children's Foundation; and the Australian Research Council (FT130100659). FACS analysis was performed at the Queensland Brain Institute, The University of Queensland, Flow Cytometry Facility. Optical microscopy was performed at the ACRF/IMB Cancer Biology Imaging Facility established with the generous support of the Australian Cancer Research Foundation.

References

[Abreu-Blanco et al., 2011] Abreu-Blanco, M. T., Verboon, J. M., & Parkhurst, S. M. (2011). Cell wound repair in Drosophila occurs through three distinct phases of membrane and cytoskeletal remodeling. *The Journal of cell biology*, *193*(3), 455-464.

[Abreu-Blanco et al., 2012] Abreu-Blanco, M. T., Verboon, J. M., Liu, R., Watts, J. J., & Parkhurst, S. M. 2012. Drosophila embryos close epithelial wounds using a combination of cellular protrusions and an actomyosin purse string. J. Cell Sci., 125, 5984–5997.

[Anon E, et al PNAS 2012] Anon, E., Serra-Picamal, X., Hersen, P., Gauthier, N. C., Sheetz, M. P., Trepat, X., & Ladoux, B. (2012). Cell crawling mediates collective cell migration to close undamaged epithelial gaps. *Proceedings of the National Academy of Sciences*, *109*(27), 10891-10896.

[Antunes et al., 2013] Antunes, M., Pereira, T., Cordeiro, J. V., Almeida L., & Jacinto, A. (2013) Coordinated waves of actomyosin flow and apical cell constriction immediately after wounding. J. Cell Biol., 202(2), 365–379.

[Brock et al., 1996] Brock, J., Midwinter, K., Lewis, J., & Martin, P. 1996. Healing of Incisional Wounds in the Embryonic Chick Wing Bud: Characterization of the Actin Purse-String and Demonstration of a Requirment for Rho Activation. J. of Cell Bio., 135(4), 1097–1107.

[Brugués et al, 2014] Brugués, A., Anon, E., Conte, V., Veldhuis, J. H., Gupta, M., Colombelli, J., ... & Trepat, X. (2014). Forces driving epithelial wound healing. *Nature Physics*.

[Buck, 1979] Buck, R.C. 1979. Cell migration in repair of mouse corneal epithelium. Inves. Ophthalmol. Visual Sci., 18(8), 767–784.

[Caldwell et al, 2014] Caldwell, B. J., Lucas, C., Kee, A. J., Gaus, K., Gunning, P. W., Hardeman, E. C., ... & Gomez, G. A. (2014). Tropomyosin isoforms support actomyosin biogenesis to generate contractile tension at the epithelial zonula adherens. *Cytoskeleton*. Cytoskeleton, 71: 663–676

[Farhadifar et al, 2007] Farhadifar, R., Röper, J. C., Aigouy, B., Eaton, S., & Jülicher, F. (2007). The influence of cell mechanics, cell-cell interactions, and proliferation on epithelial packing. *Current Biology*, *17*(24), 2095-2104.

[Fernandez-Gonzalez et al, 2009] Fernandez-Gonzalez, R., de Matos Simoes, S., Röper, J. C., Eaton, S., & Zallen, J. A. (2009). Myosin II dynamics are regulated by tension in intercalating cells. *Developmental cell*, *17*(5), 736-743.

[Fernandez-Gonzalez & Zallen, 2013] Fernandez-Gonzalez, R., & Zallen, J. A. (2013). Wounded cells drive rapid epidermal repair in the early Drosophila embryo. *Molecular biology of the cell*, *24*(20), 3227-3237.

[Fletcher et al, 2014] Fletcher, A. G., Osterfield, M., Baker, R. E., & Shvartsman, S. Y. (2014). Vertex models of epithelial morphogenesis. *Biophysical journal*, *106*(11), 2291-2304.

[Grieve & Rabouille, 2014] Grieve, A. G., & Rabouille, C. (2014). Extracellular cleavage of E-cadherin promotes epithelial cell extrusion. *Journal of cell science*, *127*(15), 3331-3346.

[Glazier & Graner, 1993] Glazier, J.A., & Graner, F. 1993. Simulation of the differential adhesion driven rearrangement of biological cells. *Phys. Rev. E.*, 47(3), 2128–2154.

[Gomez et al, 2011] Gomez GA, McLachlan RW, Yap AS. (2011) Productive tension: force-sensing and homeostasis of cell–cell junctions *Trends Cell Biol.* Sep; 21(9):499-505.

[Gomez et al, 2015] Gomez, G. A., McLachlan, R. W., Wu, S. K., Caldwell, B. J., Moussa, E., Verma, S., ... & Sap, J. (2015). An RPTPα/Src Family Kinase/Rap1 signaling module recruits Myosin IIB to support contractile tension at apical E-cadherin junctions. *Molecular Biology of the Cell*, mbc-E14.

[Graner & Glazier, 1992] Graner, F., & Glazier, J. A. 1992. Simulation of biological cell sorting using a two dimensional extended Potts model. *Phys. Rev. Lett*., 69(13), 2013–2017.

[Hales, 2001] Hales, T. C. (2001). The honeycomb conjecture. *Discrete & Computational Geometry*, *25*(1), 1-22.

[Hutson et al, 2003] M. Shane Hutson, Yoichiro Tokutake, Ming-Shien Chang, James W. Bloor, Stephanos Venakides, Daniel P. Kiehart, and Glenn S. Edwards (2003) Forces for Morphogenesis Investigated with Laser Microsurgery and Quantitative Modeling, Science 2003: 300 145-149.

[Ishimoto & Morishita, 2014] Ishimoto, Y., & Morishita, Y. (2014). Bubbly vertex dynamics: a dynamical and geometrical model for epithelial tissues with curved cell shapes. *Physical Review E*, *90*(5), 052711.

[Kabla, 2012] Kabla, A. J. (2012). Collective cell migration: leadership, invasion and segregation. *Journal of The Royal Society Interface*, rsif20120448.

[Kovacs et al, 2011] Kovacs, E. M., Verma, S., Ali, R. G., Ratheesh, A., Hamilton, N. A., Akhmanova, A., & Yap, A. S. (2011). N-WASP regulates the epithelial junctional actin cytoskeleton through a non-canonical post-nucleation pathway. *Nature Cell Biology*, *13*(8), 934-943.

[Kuipers D et al, 2014] Kuipers, D., Mehonic, A., Kajita, M., Peter, L., Fujita, Y., Duke, T., ... & Gale, J. E. (2014). Epithelial repair is a two-stage process driven first by dying cells and then by their neighbours. *Journal of Cell Science*, *127*(6), 1229-1241.

[Liang et al, 2015] Liang X., Gomez G.A. and Yap A.S. (2015) Current perspectives on cadherin-cytoskeleton interactions and dynamics. *Cell Health and Cytoskeleton*, *7* 11-24.

[Lubkov & Bar-Sagi, 2014] Lubkov, V., & Bar-Sagi, D. (2014). E-cadherin-mediated cell coupling is required for apoptotic cell extrusion. *Current Biology*, *24*(8), 868-874.

[Maître & Heisenberg, 2013] Jean-Léon Maître, Carl-Philipp Heisenberg (2013) Three functions of cadherins in cell adhesion, *Cur. Biol.* 23 R626-R633.

[Martin & Lewis, 1992] Martin, P., & Lewis, J. 1992. Actin cables and epidermal movementin embryonic wound healing. Nature, 360, 179–183.

[Martin et al, 2010] Adam C. Martin, Michael Gelbart, Rodrigo Fernandez-Gonzalez, Matthias Kaschube, and Eric F. Wieschaus (2010) Integration of contractile forces during tissue invagination *J Cell Biol.* 2010 188(5):735-49

[Mertz et al, 2013] Mertz, A. F., Che, Y., Banerjee, S., Goldstein, J. M., Rosowski, K. A., Revilla, S. F., ... & Horsley, V. (2013). Cadherin-based intercellular adhesions organize epithelial cell–matrix traction forces. *Proceedings of the National Academy of Sciences*, *110*(3), 842-847.

[Monier B. et al, 2015] Monier, B., Gettings, M., Gay, G., Mangeat, T., Schott, S., Guarner, A., & Suzanne, M. (2015). Apico-basal forces exerted by apoptotic cells drive epithelium folding. *Nature* 518, 245–248.

[Moore et al, 2014] Moore, T., Wu, SK., Michael, M., Yap, AS., Gomez, GA., & Neufeld, Z. Self-organizing actomyosin patterns on the cell cortex at epithelial cell-cell junctions. *Biophysical Journal* 107, 2652-2661.

[Nagai & Honda, 2001] Nagai, T., & Honda, H. (2001). A dynamic cell model for the formation of epithelial tissues. *Philosophical Magazine B*, *81*(7), 699-719.

[Nagai & Honda, 2009] Nagai, T., & Honda, H. (2009). Computer simulation of wound closure in epithelial tissues: Cell–basal-lamina adhesion. *Physical Review E*, *80*(6), 061903.

[Niessen et al, 2011] Niessen CM, Leckband D, Yap AS. (2011) Tissue organization by cadherin adhesion molecules: dynamic molecular and cellular mechanisms of morphogenetic regulation, *Physiol. Rev.* 91 691-731.

[Ratheesh et al., 2012] Ratheesh, A., Gomez, G. A., Priya, R., Verma, S., Kovacs, E. M., Jiang, K., … Yap, A. S. (2012). Centralspindlin and α-catenin regulate Rho signalling at the epithelial zonula adherens. *Nature Cell Biology*, *14*(8), 818–828.

[van Roy & Berx, 2008] van Roy F, Berx G. (2008) The cell-cell adhesion molecule E-cadherin Cell Mol. Life Sci. 65 3756-3788.

[Otani et al J. Cell Biol 2006] Otani, T., Ichii, T., Aono, S., & Takeichi, M. (2006). Cdc42 GEF Tuba regulates the junctional configuration of simple epithelial cells. *The Journal of Cell Biology*, *175*(1), 135-146.

[Seong et al, 2009] Seong, J., Lu, S., Ouyang, M., Huang, H., Zhang, J., Frame, M. C., & Wang, Y. (2009). Visualization of Src activity at different compartments of the plasma membrane by FRET imaging. *Chemistry & Biology*, *16*(1), 48-57.

[Shewan AM et al, 2005] Shewan, A. M., Maddugoda, M., Kraemer, A., Stehbens, S. J., Verma, S., & Kovacs, E. M. (2005). Myosin 2 is a key Rho kinase target necessary for the local concentration of E-cadherin at cell–cell contacts. *Molecular Biology of the Cell*, *16*(10), 4531-4542.

[Smutny et al, 2010] Smutny, M., Cox, H. L., Leerberg, J. M., Kovacs, E. M., Conti, M. A., Ferguson, C., ... & Yap, A. S. (2010). Myosin II isoforms identify distinct functional modules that support integrity of the epithelial zonula adherens. *Nature Cell Biology*, *12*(7), 696-702.

[Sonnemann et al, 2011] Sonnemann, K. J., & Bement, W. M. (2011). Wound repair: toward understanding and integration of single-cell and multicellular wound responses. *Annual Review of Cell and Developmental Biology*, *27*, 237-263.

[Szabo et al, 2010] Szabó, A., Ünnep, R., Méhes, E., Twal, W. O., Argraves, W. S., Cao, Y., & Czirók, A. (2010). Collective cell motion in endothelial monolayers. *Physical Biology*, *7*(4), 046007.

[Tamada et al, 2007] Tamada, M., Perez, T. D., Nelson, W. J., & Sheetz, M. P. (2007). Two distinct modes of myosin assembly and dynamics during epithelial wound closure. *The Journal of Cell Biology*, *176*(1), 27-33.

[Vedula et al, 2015] Vedula, S. R. K., Peyret, G., Cheddadi, I., Chen, T., Brugués, A., Hirata, H., Lopez-Menendez, H., Toyama, Y., de Almeida, L.N., Trepat, X., Lim, C.T. and Ladoux, B. (2015). Mechanics of epithelial closure over non-adherent environments. *Nature Communications*, *6*, 6111.

[Weber et al, 2012] Weber, G. F., Bjerke, M. A., & DeSimone, D. W. (2012). A mechanoresponsive cadherin-keratin complex directs polarized protrusive behavior and collective cell migration. *Developmental cell*, *22*(1), 104-115.

[Wu et al, 2014a] Wu SK, Gomez GA, Michael M, Verma S, Cox HL, Lefevre JG, Parton RG, Hamilton NA, Neufeld Z, Yap AS. (2014) Cortical F-actin stabilization generates apical-lateral patterns of junctional contractility that integrate cells into epithelia Nat Cell Biol. 2014 16 167-78.

[Wu et al, 2014b] Wu, Selwin K; Budnar, Srikanth; Yap, A.S; Gomez, Guillermo A (2014) Pulsatile contractility of actomyosin networks organizes the cellular cortex at lateral cadherin junctions,European Journal of Cell Biology 93 396-404.

[Wu Y et al, 2015] Wu Y, Kanchanawong P, and Zaidel-Bar R (2015) "Actin-delimited adhesion-independent clustering of E-cadherin forms the nanoscale building blocks of adherens junctions" Dev Cell 32(2):139-54.